JOURNAL OF AERONAUTICAL MATERIALS
ISSN: 1005-5053

Vol. 44, Issue-01, 2024
pp. 168-177

STUDY OF STRONG PERPENDICULAR EXCHANGE BIAS IN EPITAXIAL STRUCTURES NANOCOMPOSITES OF $LA_{0.7}SR_{0.3}MNO_3$ AND $LAFEO_3$

Rohit Kumar[1], Prof .Arun Kumar Singh[2], Dr. Deepak Kumar[3],Rakesh Chandra joshi[4]
[1]Research Scholar, Department of Physics, L.N. Mithila University, Darbhanga.
[2]Prof., University Department of Physics, L.N. Mithila University, Darbhanga.
[3]Assistant Prof., University Department of Physics, L.N. Mithila University, Darbhanga.
[4]Department of Physics, Kumaun University, Nainital, Uttrakhand
Email:-deep9435@gmail.com, rkroy190@gmail.com, singharun63@gmail.com

Abstract:- Strong exchange bias (EB) in perpendicular direction has been demonstrated in vertically aligned nanocomposite (VAN) (La0.7Sr0.3MnO3) 1−x : (LaFeO3) x (LSMO: LFO),(x = 0.33, 0.5, 0.67) thin films deposited by pulsed laser deposition. Under moderate magnetic field cooling, an EB field as high as 800 Oe is achieved in the VAN film with x = 0.33, suggesting a great potential for its applications in high-density memory devices. Such enhanced EB effects in a perpendicular direction can be attributed to the high-quality epitaxial co-growth of vertically aligned ferromagnetic LSMO and antiferromagnetic LFO phases and the vertical interface coupling associated with a disordered spin-glass state. The VAN design paves a powerful way for integrating the perpendicular EB effect within thin films and provides a new dimension for advanced spintronic devices

Keywords: Exchange bias (EB), Ferromagnet (FM), Antiferromagnet (AFM), Vertically aligned nanocomposite (VAN), X-ray diffraction (XRD, Transmission Electron Microscopy (TEM)

Introduction:-

Exchange bias (EB), referring to a shift of the magnetization hysteresis loop along the field axis, has gained great interest since its discovery in the 1950s.1 With the unidirectional magnetic anisotropy it provides, the EB effect has found critical applications in numerous spintronic devices, i.e., magnetic recording read heads and magnetic memory.2,3 The EB effect is believed to originate from the magnetic coupling across the interface shared by a ferromagnet (FM) and an antiferromagnet (AFM) when cooled in a magnetic field through the Neel temperature (TN) of the AFM.4,5 In addition to FM/AFM interfaces, this effect has also been extensively explored and reported in FM/spin-glass (SG),6–8 FM/non-magnetic interfaces,9,10, and FM/paramagnetic3 interfaces recently. Most EB effects reported in thin films are based on multilayer structures where the magnetization of the FM layer is pinned in the in-plane direction, which is parallel to the coupling interfaces. However, for next generation memories that require high thermal stability and high density, perpendicular exchange bias (PEB) is more desirable.11,12 So far, reported PEB in multilayer architectures can only be triggered in very thin FM films (less than 10 nm), found in layered noble metals Co/(Pd,Pt),13 DyCo,11 and CoFeB-based spin valves,12 which all require precise heterostructure thickness control with sophisticated facilities. In addition, in layered structures, the strength of EB is inversely proportional to the ferromagnetic layer thickness, which also hampers practical device integration. Considering that the exchange bias originates mostly from the interface coupling, it is highly expected that PEB could be derived in structures with a high density of coupling interfaces in the vertical direction.

Vertically aligned nanocomposite (VAN) thin films, in which two phases of materials can be self-assembled and grown epitaxially, provide a powerful way for vertical interface coupling and microstructure tuning14,15 and have been explored extensively for novel and enhanced functionalities, e.g., enhanced low field magnetoresistance (LFMR),16,17 superconductivity,18 and enhanced ferro- electricity,19, etc. Recently, by selecting FM La0.7Sr0.3MnO3 (LSMO) and AFM BiFeO3 as the two phases of VAN film, exchange bias in the perpendicular direction has been observed.20 In addition, with careful design of the VAN thin film growth, high density of interfaces can also be engineered to align to specific directions,21 making it promising for exploring enhanced EB in controlled orientation. Enormous opportunities in exploring new VAN materials systems, performance tunability, and the understanding of the fundamental EB mechanisms are left lacking, and thus worth Investigation.

Experiment details:-

In this work, we investigated the co-growth of FM LSMO (a = 3.87 Å, pseudo-cubic) and AFM LaFeO3 (LFO, a = 3.940 Å, pseudo-cubic) on SrTiO3 (STO, a = 3.905 Å) substrate to explore EB effect in the perpendicular direction. LFO is selected based on its good lattice matching with both STO and LSMO and the large magnetic anisotropy.22 Strong exchange bias (EB) effect in the perpendicular orientation has been achieved and can be modulated by the strain tuning effect with composition variation. Detailed microstructure and magnetic properties analysis suggest that the exchange coupling at the vertical LSMO/LFO interfaces associated with an SG state is responsible for the pronounced PEB properties here

Result and Discussion:-

(LSMO)1−x:(LFO)x nanocomposite films (with a film thickness of 1000 nm), with x = 0.33, 0.5, 0.67, were grown on single crystalline STO (001) substrates by pulsed laser deposition. The composite targets were prepared with a conventional ceramic sintering process from high-purity stoichiometric La2O3, SrCO3, MnO2, and Fe2O3 powders. During deposition, a substrate temperature of 800 ◦C and oxygen pressure of 200 mTorr were maintained. A KrF excimer laser (λ = 248 nm) with a repetition rate of 10 Hz was used. All films were cooled at 10 ◦C/min under 200 Torr O2 after deposition. X-ray diffraction (XRD) (PAN Analytical Empyrean XRD) and transmission electron microscopy (TEM) (FEI Tecnai G2 F20 operated at 200 kV) were used to analyze the crystallinity and microstructure of the films.

The out-of-plane magnetizations of the films were measured by a commercial Physical Property Measurement System (PPMS Model 6000, Quantum Design) with a Vibrating Sample Magnetometer (VSM). The temperature-dependent magnetization (M-T) data were collected during the heating cycle, after cooling down the samples from 350 K to 5 K with (field-cooling, FC) or without (zero-field-cooling, ZFC) applied magnetic field. Hysteresis loops were obtained after cooling the sample from 300 K under a specific magnetic field (Hcool) down to the desired temperature.

Fig. 1(a) shows XRD θ-2θ plots of the pure LSMO and LSMO: LFO nanocomposite films. Both LSMO and LFO phases grow highly textured along (00l) on STO substrate without any obvious impurity peak. To further investigate the crystal structure and the strain states of the composite films, reciprocal space mapping (RSM) were performed near the (113) STO peak.

Figs. 1(c) and 1(d) shows typical RSMs for LSMO0.67LFO0.33 and LSMO0.33LFO0.67, respectively. Both of them show clearly separated LSMO (113) and LFO (113) peak, suggesting highly epitaxial two phase co-growth in the films. In addition, it is interesting to note that the LSMO and LFO peaks present minor spread in the out-of-plane direction, suggesting small or no strain relaxation through the thickness of the film, which is consistent with the general feature of VAN films, i.e., the strain state is dominated by the strain coupling across the hetero-interfaces between the two phases in the vertical direction rather than by the STO substrate for thick film.19,21,23,24 A Strong strain tuning effect exists as the LSMO and LFO peaks shift systematically with the composition variation. The calculated out-of-plane lattice parameters of LSMO are plotted in Fig. 1(b) and summarized in Table I. The vertical strain state of LSMO was converted from compressive (0.17%) for x = 0 to tensile (+1.3%) for x = 0.67, which is expected from the interface strain coupling between LSMO (a = 3.87 Å, pseudo cubic) and LFO (a = 3.94 Å, pseudo cubic).

Detailed microstructure analysis was conducted via TEM and scanning transmission electron microscopy (STEM) for the composite films, as shown in Fig. 2. Fig. 2(a) displays a typical cross-section TEM image of the LSMO0.67LFO0.33 film, showing vertically self-assembled two-phase growth with columnar structures on the substrate, further evidenced by the energy-dispersive X-ray spectroscopy (EDX) results (inset of Fig. 2(a)) taken under the STEM mode. The EDX line scan shows alternating Mn-rich and Fe-rich regions, corresponding to the columnar LSMO phase and LFO phase. High-resolution TEM images (Fig. S144 of the supplementary material)

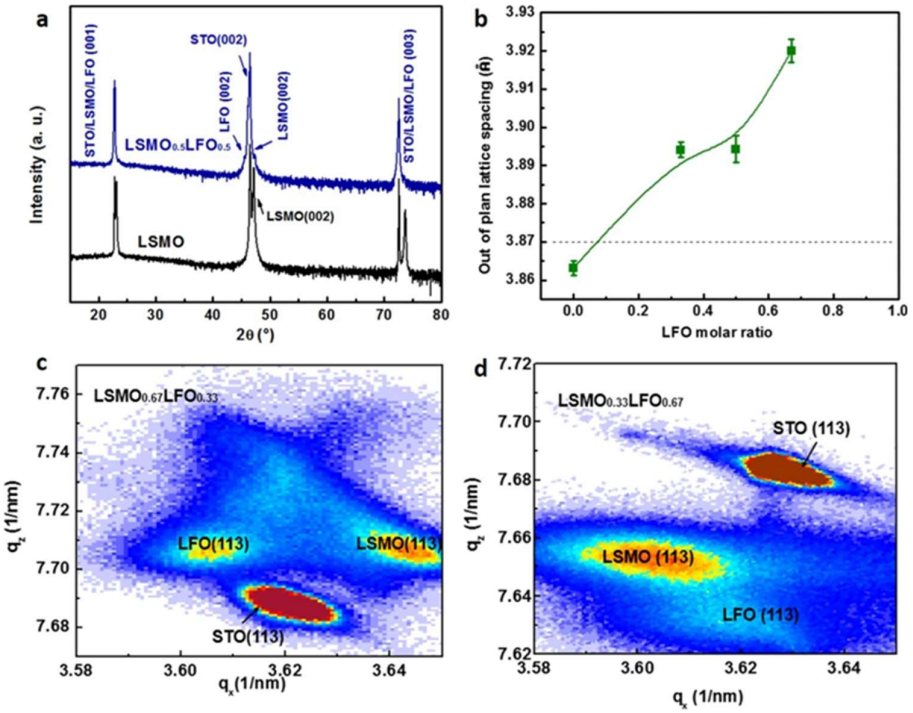

FIG. 1. (a) XRD θ-2θ plots of pure LSMO and the LSMO0.5LFO0.5 nanocomposite films. (b) Out-of-plane lattice parameter of LSMO with different LFO molar ratios. Reciprocal space maps near STO (113) of (c) LSMO0.67LFO0.33 and (d) LSMO0.33LFO0.67.

indicate one-to-one lattice matching between LSMO and LFO, expected from the small calculated lattice mismatch (1.7%). Plan-view TEM image of LSMO0.5LFO0.5 (Fig. 2(c)) shows LFO phases embedded in the LSMO matrix, with domain diameter of 2-10 nm. Figs. 2(b) and 2(d), and inset of Fig. 2(d) are the TEM, STEM image and the selected area electron diffraction (SAED) pattern of LSMO0.33LFO0.67 film, respectively. The bright and dark columns in the STEM im- age correspond to the LFO (brighter contrast) and LSMO (darker contrast) phases. LFO domain diameter is determined to be less than 10 nm also. Distinguished diffraction dots in the SAED pattern indicate high epitaxial quality of the composite film. Both LSMO and LFO grow cube-on- cube on STO substrate, with the lattice matching relations of (002)LSMO//(002)LFO//(002)STO and (020)LSMO//(020)LFO//(020)STO.

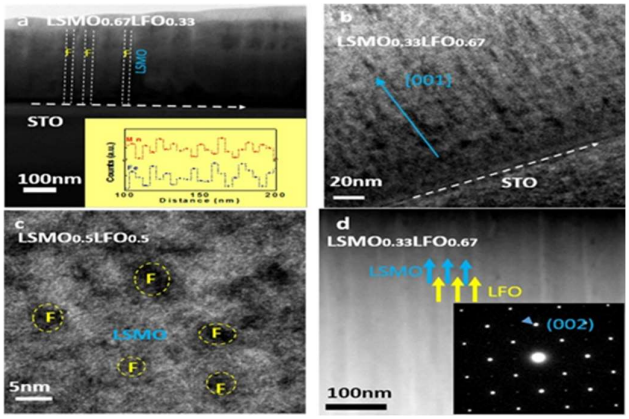

fig. 2. Self-assembled vertically aligned nanostructures of (LSMO)1−x:(LFO)x VAN films. (a) Cross-sectional TEM image of the LSMO0.67LFO0.33 nanocomposite film. Inset of (a) EDS line scan results across several pillars. (b) Cross-sectional TEM image of LSMO0.33LFO0.67 VAN film. (c) Plan-view TEM image of LSMO0.5LFO0.5 sample showing LFO nanopillars embedded in LSMO matrix. F indicates LFO. (d) Cross-sectional STEM image and diffraction pattern (inset of (d)) of LSMO0.33LFO0.67.

Magnetic properties

Magnetic properties of the films were analyzed using PPMS with VSM. After field cooling process starting from 300 K, which is well below TN of LFO (∼740 K),25 obvious PEB effect was observed at 5 K for all the (LSMO)1−x:(LFO)x films, while pure LSMO film showing no obvious EB effect. Fig. 3(a) shows a typical magnetic hysteresis loop of the LSMO0.67LFO0.33 film at 5 K after field cooling under 1 T. It is obvious that the hysteresis loop shifted to the left along the magnetic field axis, which is opposite to the cooling field direction. The EB field HEB and coercive field Hc are calculated using HEB = H1 + H2 /2 and Hc = H1 H2 /2, where H1 and H2 are negative and positive fields at which the magnetization equals zero, respectively. A large EB field of 690 Oe was derived, accompanied with a coercive field Hc of 1600 Oe. A training effect has also been observed with the fifth scan of the hysteresis loop giving a HEB of 545 Oe. Similar EB behavior also shows up with smaller magnitudes of HEB for VAN films of x = 0.5 and 0.67 (not shown here). Both the horizontal shift of the hysteresis loop and the coercivity enhancement correspond to the characteristic features of the exchange bias,4,5 indicating robust exchange coupling at the vertical direction in the VAN systems. The EB phenomenon here is much stronger compared toreported LSMO

based multilayers/nanostructures, which is typically less than 300 Oe,26–29 and also comparable with (LSMO)1−x: BiFeO3 x nanocomposite, in which a 1000 Oe shift was observed for x = 0.25.20

To understand the PEB effect here, M-T behavior measured in 1000 Oe of the films has been investigated and plotted in Fig. 3(b). Systematic modulation can be seen: The magnetization of the nanocomposite films reduces in the entire temperature regime with increasing LFO concentration and consists of the FM LSMO volume ratio.30 The ferromagnetic transition temperature is

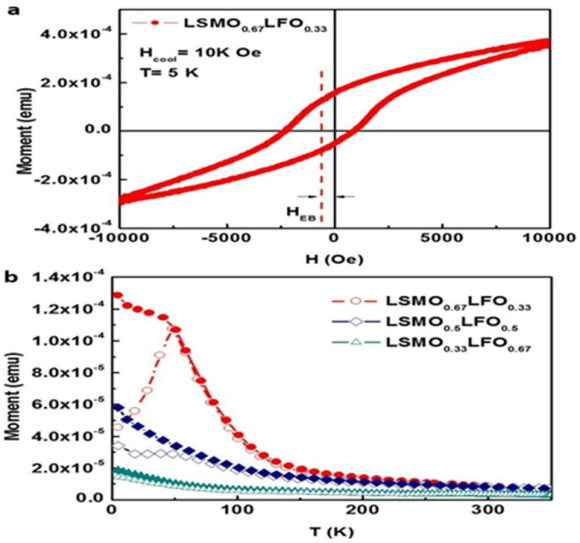

FIG. 3. (a) Magnetization hysteresis curves of LSMO0.67LFO0.33 VAN film measured at 5 K after field cooling in +1 T, (b) field cooling, and zero-field cooling magnetization versus temperature plots for (LSMO)1−x(LFO)x VAN films.

Derived to be 200 K, 150 K, and 50 K for x = 0.33, 0.5, and 0.67, respectively, which can be linked to strain tuning and phase boundary effect in the VAN films: As shown in Table I, with increasing LFO molar ratio, LSMO mosaic spreads in the out-of-plane directions, which could impact on the Mn–O–Mn bond length and angle, thus affecting the exchange energy.31,32 In addition, insulating AFM LFO embedded in LSMO matrix could serve as energy barriers among LSMO domains, suppressing the long-range double exchange interaction.16

A peak at Tp in ZFC M-T curves and obvious bifurcation below temperature Tirr between the ZFC and FC curves have been observed. It has been reported that such features mostly suggest a disordered spin-glass (SG) state,20,26,33 where Tp is close to Tirr,26 and different with superparamagnetic systems where the magnetization of FC increases monotonously with decreasing tempera- ture.28,34 For this case, the SG state can be linked to the competition of the FM double-exchange and AFM super-exchange couplings at the LSMO/LFO interfaces. As known, the G-type AFM order in LaFeO3 is not expected to pin the LSMO FM spins because of its fully compensated spin arrangement at the interfaces,27,35,36 and the perfect one-to-one lattice matching epitaxy between LSMO and LFO suggests that the interfacial defects effect can be neglected. We thus ascribe the EB behavior here to be correlated with the interfacial SG state, similar with that discussed in previous reports with La0.7Sr0.3MnO3:SrMnO3,28 La0.7Sr0.3MnO3:LaSrMnO426 layered structures, etc. In the

(LSMO)1−x:(LFO)x films, after cooling under an applied magnetic field along the vertical direction, frozen FM spins can be induced at the SG interfaces, giving an additional torque on the LSMO

FM spins, which the external field has to overcome when flipping. To further confirm the role of the frozen FM spins at the interfaces,37 the ZFC M-T curve at high magnetic field of 1 T (shown

in Fig. 2a44 of the supplementary material) and temperature dependent HEB (Fig. 2b44) were investigated. For LSMO0.67LFO0.33, the HEB decreases to 0 at 20 K and consists well with the spin freezing temperature (Tf) estimated from the M-T curve.

The dependency of HEB (4a) and Hc (4b) on cooling field (Hcool) gives further evidence, supporting the role of the interfacial frozen spins associated with the SG in the PEB. The data were collected after field cooling from 300 K to 5 K. The HEB increases with increasing Hcool initially and then decreases gradually, and the Hc increases in the entire regime under investigation. This behavior normally occurs at FM/AFM interface associated with disordered SG moments, which could be frozen at low temperatures,26,33,38,39 as reported in FM-AFM multilayer,38 cluster-glass compounds such as La1−xSrxCoO3,40 Fe nanoparticles embedded in iron oxide matrix,39 etc. The initial increase of HEB could be explained by increased exchange coupling resulted from the larger number of interfacial spins frozen in the field direction. The decrease of HEB under high magnetic field may be correlated with the Zeeman coupling effect,27,39 which can compete with interfacial exchange coupling.

Last, composition modulated PEB can be observed in Fig. 4, showing HEB x = 0.33 > HEB x = 0.67 > HEB (x = 0.5) in the investigated region. This behavior might be linked with the strain states in the systems, because of the critical role of strain on determining the spin frustration states.28,31,41 For FM/G-type AFM, the spin frustration at the interface can occur in both AFM and FM phases,28 thus depends on both the LSMO and LFO strain status and their interfacial strain. Previous reports suggest that larger strain in LSMO or LFO and smaller interfacial strain can lead to stronger spin frustration in the system.28,30,31,41

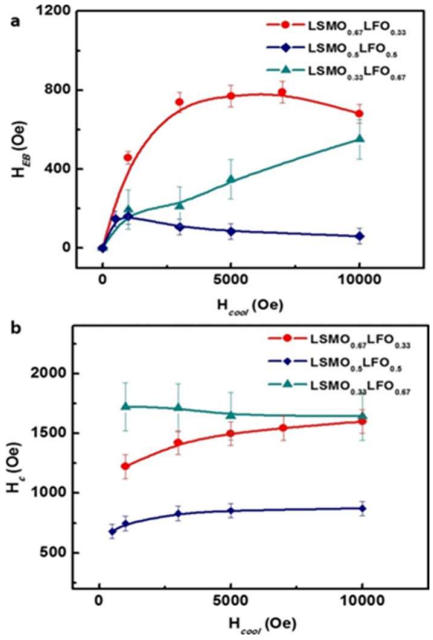

Fig:4 cooling field effect on the exchange bias behavior. (a) HEB and (b) Hc of (LSMO)1−x:(LFO)x VAN films as a function of the cooling field

Conclusion:-

41 As summarized, it can be expected that sample of x = 0.33 and 0.67 exhibit stronger spin frustration than that of x = 0.5, due to the large LFO strain (1.16%) and small interfacial strain (0.025%) for x = 0.33, and large LSMO strain (1.3%) together with 0.24% interfacial strain for x = 0.67. While sample of x = 0.5 has a small strain for both LSMO (0.64%) and LFO (0.76%) and a larger interfacial strain (0.38%), making both LSMO FM and LFO AFM state stable and a weak spin frustration across the interface. As is expected that systems with stronger disorder-induced frustration will support greater ex- change bias,6,42 the strain induced spin disorder consist well with the observed experimental results, i.e., HEB x = 0.33 > HEB x = 0.67 > HEB x = 0.5 . In addition, the slightly larger LFO pillar size (12 nm) in LSMO0.67LFO0.33 might also contribute to the enhancement of the HEB in it, as HEB usually increases with SG-thickness (tSG) initially and then saturates.6,8,43 Future experiments are needed to explore the distance-dependent magnetic profiles at the interface to get the idea of the thickness and spin states in the disordered region.

Using unique vertically aligned nanocomposite structure design, we have demonstrated highly textured (LSMO)1−x:(LFO)x films grown on STO substrates. By confining the FM/AFM heterointerfaces in the vertical direction, significant exchange bias in the out-of-plane direction for micrometer-thick VAN films has been observed, which is promising for advanced spintronic devices application. Detailed microstructure and magnetic property analysis suggest that the disordered spin-glass states at the LSMO/LFO interfaces related to magnetic frustration are responsible for the EB effect, with the interfacial frozen spins giving an additional torque on the LSMO FM spins. Systematic property modulation can be achieved by strain tuning effect with composition control.

Acknowledgment:-

At Indore's UGC-DAE Consortium for Scientific Research, magnetic measurements were carried out. The writers sincerely appreciate the insightful conversation with Dr. Ram Janay Choudhary of UGC-DAE, CSR Indore. The authors express their sincere gratitude to Dr. Simant Kumar Srivastava of the University of Allahabad's Department of Chemistry for providing the research facilities used in this study.

Reference:-

1. W. H. Meiklejohn and C. P. Bean, “New magnetic anisotropy,” Phys. Rev. 102, 1413 (1956).
2. J. Nogués and I. K. Schuller, “Exchange bias,” J. Magn. Magn. Mater. 192, 203–232 (1999).
3. M. Gibert, P. Zubko, R. Scherwitzl, J. Íñiguez, and J.-M. Triscone, “Exchange bias in LaNiO3–LaMnO3 superlattices,” Nat. Mater. 11, 195–198 (2012).
4. M. Kiwi, “Exchange bias theory,” J. Magn. Magn. Mater. 234, 584–595 (2001).

5. J. Nogués, J. Sort, V. Langlais, V. Skumryev, S. Suriñach, J. S. Muñoz, and M. D. Baró, "Exchange bias in nanostructures," Phys. Rep. 422, 65–117 (2005).
6. M. Ali, P. Adie, C. H. Marrows, D. Greig, B. J. Hickey, and R. L. Stamps, "Exchange bias using a spin glass," Nat. Mater.6, 70–75 (2007).
7. F. Te Yuan, J. K. Lin, Y. D. Yao, and S. F. Lee, "Exchange bias in spin glass (FeAu)/NiFe thin films," Appl. Phys. Lett. 96, 18–21 (2010).
8. K. D. Usadel and U. Nowak, "Exchange bias for a ferromagnetic film coupled to a spin glass," Phys. Rev. B 80, 014418(2009).
9. Y. Fan, K. J. Smith, G. Lüpke, A. T. Hanbicki, R. Goswami, C. H. Li, H. B. Zhao, and B. T. Jonker, "Exchange bias of the interface spin system at the Fe/MgO interface," Nat. Nanotechnol. 8, 438–444 (2013).
10. S. J. Zhu, J. Yuan, B. Y. Zhu, F. C. Zhang, B. Xu, L. X. Cao, X. G. Qiu, B. R. Zhao, and P. X. Zhang, "Exchange bias effect
11. and enhanced magnetoresistance in La0.67Sr0.33MnO3/SrTiO3 superlattices," Appl. Phys. Lett. 90, 112502 (2007).
12. F. Radu, R. Abrudan, I. Radu, D. Schmitz, and H. Zabel, "Perpendicular exchange bias in ferrimagnetic spin valves," Nat.Commun. 3, 715 (2012).
13. S. Ikeda, K. Miura, H. Yamamoto, K. Mizunuma, H. D. Gan, M. Endo, S. Kanai, J. Hayakawa, F. Matsukura, and H. Ohno, "A perpendicular-anisotropy CoFeB-MgO magnetic tunnel junction," Nat. Mater. 9, 721–724 (2010).
14. S. Maat, K. Takano, S. Parkin, and E. Fullerton, "Perpendicular exchange bias of Co/Pt multilayers," Phys. Rev. Lett. 87,87202 (2001).
15. W. Zhang, R. Ramesh, J. L. MacManus-Driscoll, and H. Wang, "Multifunctional, self-assembled oxide nanocomposite thin films and devices," MRS Bull. 40, 736–745 (2015).
16. J. L. MacManus-Driscoll, A. Suwardi, and H. Wang, "Composite epitaxial thin films: A new platform for tuning, probing,and exploiting mesoscale oxides," MRS Bull. 40, 933–942 (2015).
17. M. Fan, W. Zhang, F. Khatkhatay, L. Li, and H. Wang, "Enhanced tunable magnetoresistance properties over a wide temper- ature range in epitaxial La0.7Sr0.3MnO3 1 x: CeO2 x nanocomposites," J. Appl. Phys. 118, 065302 (2015).
18. W. Zhang, A. Chen, F. Khatkhatay, C. Tsai, Q. Su, L. Jiao, X. Zhang, and H. Wang, "Integration of self-assembled vertically
19. aligned nanocomposite La0.7Sr0.3MnO3 1−x:(ZnO)x thin films on silicon substrates," ACS Appl. Mater. Interfaces 5, 3995 (2013).J. Huang, C.-F. Tsai, L. Chen, J. Jian, F. Khatkhatay, K. Yu, and H. Wang, "Magnetic properties of (CoFe2O4)x:(CeO2)1−x vertically aligned nanocomposites and their pinning properties in YBa2Cu3O7−δ thin films," J. Appl. Phys. 115, 123902 (2014).
20. S. A. Harrington, J. Zhai, S. Denev, V. Gopalan, H. Wang, Z. Bi, S. A. T. Redfern, S.-H. Baek, C. W. Bark, C.-B. Eom, Q. Jia, M. E. Vickers, and J. L. Macmanus-Driscoll, "Thick lead-free ferroelectric films with high Curie temperatures through nanocomposite-induced strain," Nat. Nanotechnol. 6, 491–495 (2011).
21. W. Zhang, A. Chen, J. Jian, Y. Zhu, L. Chen, P. Lu, Q. Jia, J. L. MacManus-Driscoll, X. Zhang, and H. Wang, "Strong perpendicular exchange bias in epitaxial

La0.7Sr0.3MnO3:BiFeO3 nanocomposite films through vertical interfacial coupl- ing," Nanoscale 7, 13808 (2015).

22. W. Zhang, M. Fan, L. Li, A. Chen, Q. Su, Q. Jia, J. L. MacManus-Driscoll, and H. Wang, "Heterointerface design and strain tuning in epitaxial BiFeO3:CoFe2O4 nanocomposite films," Appl. Phys. Lett. 107, 212901 (2015).

23. T. Fujii, I. Matsusue, and J. Takada, "Superparamagnetic behaviour and induced ferrimagnetism of LaFeO3 nanoparticles prepared by a hot-soap technique," in Advanced Aspects of Spectroscopy (InTech, 2012).

24. W. Zhang, A. Chen, Z. Bi, Q. Jia, J. L. Macmanus-Driscoll, and H. Wang, "Interfacial coupling in heteroepitaxial vertically aligned nanocomposite thin films: From lateral to vertical control," Curr. Opin. Solid State Mater. Sci. 18, 6–18 (2014).

25. S. Lee, W. Zhang, F. Khatkhatay, Q. Jia, H. Wang, and J. L. Macmanus-Driscoll, "Strain tuning and strong enhancement of ionic conductivity in SrZrO3-RE2O3 (RE = Sm, Eu, Gd, Dy, and Er) nanocomposite films," Adv. Funct. Mater. 25, 4328–4333 (2015).

26. F. Nolting, A. Scholl, J. Stöhr, J. W. Seo, J. Fompeyrine, H. Siegwart, J.-P. Locquet, S. Anders, J. Lüning, E. E. Fuller- ton, M. F. Toney, M. R. Scheinfein, and H. A. Padmore, "Direct observation of the alignment of ferromagnetic spins by antiferromagnetic spins," Nature 405, 767–769 (2000).

27. B. Cui, C. Song, G. Y. Wang, H. J. Mao, F. Zeng, and F. Pan, "Strain engineering induced interfacial self-assembly and intrinsic exchange bias in a manganite perovskite film," Sci. Rep. 3, 2542 (2013).

28. T. Yu, X. K. Ning, W. Liu, J. N. Feng, X. G. Zhao, and Z. D. Zhang, "Exchange bias effect in epitaxial La0.67Ca0.33MnO3/SrMnO3 thin film structure," J. Appl. Phys. 116, 083908 (2014).

29. J. F. Ding, O. I. Lebedev, S. Turner, Y. F. Tian, W. J. Hu, J. W. Seo, C. Panagopoulos, W. Prellier, G. Van Tendeloo, and T. Wu, "Interfacial spin glass state and exchange bias in manganite bilayers with competing magnetic orders," Phys. Rev. B87, 054428 (2013).

30. X. K. Ning, Z. J. Wang, X. G. Zhao, C. W. Shih, and Z. D. Zhang, "Exchange bias in La0.7Sr0.3MnO3/NiO and LaMnO3/NiO interfaces," J. Appl. Phys. 113, 223903 (2013).

31. X. Ning, Z. J. Wang, X. Zhao, C. Shih, W. Chang, and Z. Zhang, "Exchange bias effect and magnetic properties in La0.7Sr0.3MnO3-NiO nanocomposite films," IEEE Trans. Magn. 50, 1–4 (2014).

32. C. Adamo, X. Ke, H. Q. Wang, H. L. Xin, T. Heeg, M. E. Hawley, W. Zander, J. Schubert, P. Schiffer, D. A. Muller, L.Maritato, and D. G. Schlom, "Effect of biaxial strain on the electrical and magnetic properties of (001) La0.7Sr0.3MnO3 thin films," Appl. Phys. Lett. 95, 112504 (2009).

33. D. Pesquera, G. Herranz, A. Barla, E. Pellegrin, F. Bondino, E. Magnano, F. Sánchez, and J. Fontcuberta, "Surface symmetry-breaking and strain effects on orbital occupancy in transition metal perovskite epitaxial films," Nat. Commun. 3, 1189 (2012).

34. M. Patra, K. De, S. Majumdar, and S. Giri, "Exchange bias with Fe substitution in LaMnO3," Eur. Phys. J. B 58, 367–371 (2007).

35. J. Alonso, M. L. Fdez-Gubieda, J. M. Barandiarán, A. Svalov, L. Fernández Barquín, D. Alba Venero, and I. Orue, "Crossover from superspin glass to superferromagnet in FexAg100 x nanostructured thin films (20 x 50)," Phys. Rev. B 82, 054406 (2010).

36. Y. Takamura, E. Folven, J. B. R. Shu, K. R. Lukes, B. Li, A. Scholl, A. T. Young, S. T. Retterer, T. Tybell, and J. K. Grepstad, "Spin-flop coupling and exchange bias in embedded complex oxide micromagnets," Phys. Rev. Lett. 111, 107201 (2013).
37. P. Yu, J. S. Lee, S. Okamoto, M. D. Rossell, M. Huijben, C. H. Yang, Q. He, J. X. Zhang, S. Y. Yang, M. J. Lee, Q. M. Ramasse, R. Erni, Y. H. Chu, D. A. Arena, C. C. Kao, L. W. Martin, and R. Ramesh, "Interface ferromagnetism and orbital reconstruction in BiFeO3-La0.7Sr0.3MnO3 heterostructures," Phys. Rev. Lett. 105, 027201 (2010).
38. Q. K. Ong, A. Wei, and X. M. Lin, "Exchange bias in Fe/Fe3O4 core-shell magnetic nanoparticles mediated by frozen interfacial spins," Phys. Rev. B 80, 134418 (2009).
39. W. B. Rui, Y. Hu, A. Du, B. You, M. W. Xiao, W. Zhang, S. M. Zhou, and J. Du, "Cooling field and temperature dependent exchange bias in spin glass/ferromagnet bilayers," Sci. Rep. 5, 13640 (2015).
40. L. Del Bianco, D. Fiorani, A. M. Testa, E. Bonetti, and L. Signorini, "Field-cooling dependence of exchange bias in a granular system of Fe nanoparticles embedded in an Fe oxide matrix," Phys. Rev. B 70, 052401 (2004).
41. Y. K. Tang, Y. Sun, and Z. H. Cheng, "Exchange bias associated with phase separation in the perovskite cobaltite La1−xSrxCoO3," Phys. Rev. B 73(17), 174419 (2006).O. Gomonay and I. Lukyanchuk, "Magnetostriction-induced anisotropy in the exchange biased bilayers," Metallofiz. I Noveishie Technol. 36, 1453–1464 (2014); arXiv:1404.1591.
42. M. Ali, C. Marrows, and B. Hickey, "Onset of exchange bias in ultrathin antiferromagnetic layers," Phys. Rev. B 67, 172405 (2003).
43. K. T. Y. Kung, L. K. Louie, and G. L. Gorman, "MnFe structure-exchange anisotropy relation in the NiFe/MnFe/NiFe system," J. Appl. Phys. 69, 5634–5636 (1991).
44. See supplementary material at http://dx.doi.org/10.1063/1.4958965 for detailed High-resolution TEM images and temper- ature dependent HEB behavior analysis